Food & Function

ROYAL SOCIETY OF CHEMISTRY

PAPER

View Article Online
View Journal | View Issue

Cite this: *Food Funct.*, 2025, **16**, 5105

Impact of mucin protein corona on the gastrointestinal behavior and antioxidant activity of food carbon dots extracted from bread crust†

Shichao Mi,[a] Zimo Liu,[a] Mingcheng Wang,[a] David Julian McClements,[c] Chongjiang Cao,[a] Xiao Xu *[b] and Biao Yuan *[a]

Bread products are widely consumed around the globe as they are a staple food in many countries. Recent studies have shown that the elevated temperatures and prolonged times used during bread baking can lead to the formation of appreciable amounts of carbon dots, which may have adverse effects on human health. Consequently, it is important to elucidate the potential fate of these carbon dots within the gastrointestinal tract. In this study, we characterized the properties of bread-derived carbon dots (BDCDs) and then investigated their interactions with mucin. The average diameter of the individual BDCDs was 5.81 nm but they tended to exist as clusters (around 91 nm) in aqueous environments. The BDCDs mainly consisted of carbon (70.9%), oxygen (27.6%), and nitrogen (1.5%). Like other types of carbon dots, the BDCDs were found to exhibit natural fluorescence. In simulated saliva, the carbon dots interacted with mucin to form BDCD–mucin complexes. These interactions caused the zeta potential of the BDCDs to change from −5.97 to −11.07 mV and their hydrodynamic diameters to increase from 91.3 to 122.4 nm. Moreover, these interactions caused changes in the conformation of the mucin. Furthermore, *in vitro* simulated digestion studies showed that the BDCDs induced conformational changes in pepsin, reducing its enzymatic activity by around 20.8%. However, this effect was mitigated when BDCD–mucin complexes were used instead of BDCDs, highlighting the important role that mucin plays in mediating carbon dot–enzyme interactions. Moreover, the BDCD–mucin complexes were better at attenuating reactive oxygen species generation in Caco-2 cells than BDCDs, which led to higher cell viability. This study provides new insights into the role of mucin coronas in modulating the gastrointestinal behavior of carbon dots, highlighting their potential impact on human health.

Received 6th January 2025,
Accepted 5th May 2025

DOI: 10.1039/d5fo00088b

rsc.li/food-function

1. Introduction

Carbon dots are a class of carbon-based nanoparticles, ranging in size from 4 to 30 nm, that are widely used in many fields due to their high fluorescence, photostability, and solubility.[1,2] The preparation of carbon dots for various applications has been a prominent research area for many years. Recently, however, particular attention has been paid to the presence of carbon dots in different food sources, especially regarding their potential health risks.[3] Carbon dots have been reported to form during the thermal processing of some foods, especially those that are held at high temperatures for prolonged times, which is the case for products such as bread, hot beverages, and roasted meats.[4–6] The high temperatures (175–190 °C) and extended times (20–60 min) used during baking provide optimal conditions for the formation of carbon dots in bread crust, particularly darker colored ones. The carbon dots in bread crust may therefore be readily ingested as part of the daily human diet. Given the widespread presence of carbon dots in bread crust, their potential effects *in vivo* are non-negligible. Previous studies have shown that carbon dots derived from roasted squid can accumulate in various organs of mice in a time-dependent manner after ingestion, including crossing the blood–brain barrier and entering the brain.[7] Furthermore, research has shown that these carbon dots can induce cell membrane damage, cell cycle arrest, mitochondrial dysfunction, and ROS production in cells.[8] Consequently, it is important to better understand the potential gastrointestinal fate of carbon dots from bread.

[a]*Department of Food Quality and Safety, National R&D Center for Chinese Herbal Medicine Processing, College of Engineering, China Pharmaceutical University, Nanjing, Jiangsu 211198, China. E-mail: yuanbiao01@gmail.com, yuanbiao@cpu.edu.cn*
[b]*School of Life Science, Shaoxing University, Shaoxing, Zhejiang 312000, China. E-mail: xiaolexu@126.com*
[c]*Department of Food Science, University of Massachusetts, Amherst, MA 01003, USA*
†Electronic supplementary information (ESI) available. See DOI: https://doi.org/10.1039/d5fo00088b

Mucin is a highly glycosylated protein that forms a porous gel-like coating around the walls of the gastrointestinal tract, and is present in the gastrointestinal fluids.[9] It is secreted by goblet cells to form a protective mucus layer, serving as a barrier that protects intestinal epithelial cells from mechanical and physical damage while allowing nutrient absorption.[10] Previous studies have shown that mucin can also adsorb onto the surfaces of nanoparticles to form a coating around them, which is often referred to as the 'protein corona' (even though it also contains other constituents), which alters their gastrointestinal fate.[11] Zhou *et al.* reported that the formation of a mucin corona around TiO_2 nanoparticles in simulated salivary fluids impacted the dispersion state of TiO_2 nanoparticles.[12] This change in the oral dispersion state influences their subsequent behavior in the lower regions of the gastrointestinal tract. Other researchers reported that the formation of a mucin corona around transferrin-modified nanoparticles enhanced their endocytosis and transcellular transport.[13] In our previous study, we showed that the formation of a whey protein corona around TiO_2 nanoparticles altered their aggregation state and surface charge under simulated gastrointestinal conditions.[14,15] Despite these studies, there is still a relatively poor understanding of the impact of corona formation on the gastrointestinal fate of different kinds of nanoparticles.[16] In this study, we therefore examined the impact of mucin corona formation on the behavior of carbon dots under simulated gastrointestinal conditions.[17,18]

Previously, it has been shown that nanoparticles can interact with digestive enzymes in the gastrointestinal tract, which may impact their activity. For instance, Song *et al.* reported that food-derived carbon dots could interact with pepsin to form protein coronas, which decreased the activity of pepsin in simulated gastric fluids.[5] These alterations in digestive enzyme activity after interacting with the nanoparticles may be due to changes in the secondary structure of the enzymes after they adsorb onto the particle surfaces.[19] Carbon dots with different functional groups have been reported to affect digestive enzyme activity to varying degrees due to the structural modifications induced by these functional groups.[20] Interestingly, some researchers have found that interactions between nanoparticles and digestive enzymes actually enhance their activities.[21] For instance, the formation of a protein corona consisting of α-amylase and amylopsin around quercetin-protein nanoparticles increased the enzyme activity in simulated salivary and intestinal fluids, respectively, which was attributed to alterations in the secondary structure of these digestive enzymes.[22] In contrast, it has been reported that the formation of a pepsin corona around chitin nanowhiskers caused little change in the activity of pepsin, despite variations in its secondary structure.[23] Nevertheless, previous studies have overlooked the presence of mucin in the gastrointestinal tract, which may impact the effects of carbon dots on digestive enzymes.

In the present study, bread-derived carbon dots (BDCDs) were first characterized, and then their interactions with mucin were investigated. The impact of the BDCD–mucin interactions on the secondary structure and optical properties of the mucin was also studied. An *in vitro* simulated digestion model was then used to explore the impact of the mucin corona on the behavior of the BDCDs in the gastrointestinal tract. The impact of BDCDs and BDCD–mucin complexes on the activity of digestive enzymes, particularly pepsin, was also determined, so as to elucidate the role of the mucin. The antioxidant activity of the BDCD–mucin complexes during simulated digestion was studied using radical scavenging assays, as well as a reducing power assay. Furthermore, the effects of the BDCD–mucin complexes on cell viability and reactive oxygen species levels were evaluated using a cell culture model. Overall, our findings reveal that mucin in the gastrointestinal tract modulates the behavior and antioxidant activity of BDCDs through the formation of a corona around them, thereby providing a novel perspective for assessing their safety and functionality.

2. Materials and methods

2.1. Materials

The bread crust used in this study was obtained from commercially available toast bread, whose primary ingredients included wheat flour, white granulated sugar, vegetable oil, egg pulp, and milk powder (Shenyang Taoli Bread Co., Ltd, Taoli, Shenyang, China). Dialysis bags with a molecular weight cut-off of 3500 Da and 500 Da were obtained from Viskase (Chicago, USA). Mucin (≥95%), α-amylase (≥95%, from *Bacillus licheniformis*, exhibits catalytic activity comparable to human salivary α-amylase, albeit with physiologically relevant limitations), pepsin (EC 3.4.23.1, ≥95%, from porcine gastric mucosa), trypsin (EC 3.4.21.4, ≥95%, from porcine pancreas), and iron(II) sulfate heptahydrate ($FeSO_4{\cdot}7H_2O$, ≥99.7%) were obtained from Shanghai Macklin Biochemical Technology Co., Ltd (Shanghai, China). Bile salt (≥95%), benzoyl-L-arginine ethyl ester ($C_{15}H_{22}N_4O_3{\cdot}HCl$, 98%), potassium persulfate ($K_2S_2O_8$, ≥99.5%), and potassium ferrocyanide trihydrate ($K_4FeC_6N_6{\cdot}3H_2O$, 98%) were purchased from Aladdin Chemical Reagent Co., Ltd (Shanghai, China). Methanol (CH_4O, ≥99.7%) and salicylic acid ($C_7H_6O_3$, ≥99.7%) was purchased from General Reagent Co., Ltd (Shanghai, China). 3-(4,5-Dimethyl-2-thiazolyl)-2,5-diphenyl-2-*H*-tetrazolium bromide (MTT, 98%) and a ROS assay kit were purchased from Beyotime Biotechnology (Shanghai, China). Bovine hemoglobin (≥95%) and ABTS ($C_{18}H_{24}N_6O_6S_4$, 98%) were purchased from Yuanye Biotechnology Co., Ltd (Shanghai, China). Trichloroacetic acid ($C_2HCl_3O_2$, ≥99.7%) and ferric chloride ($FeCl_3{\cdot}6H_2O$, ≥99.7%) were purchased from Shanghai Hushi Laboratory Equipment Co., Ltd (Shanghai, China). Hydrogen peroxide (H_2O_2, 30%) was purchased from Nanjing Chemical Reagent Co., Ltd (Nanjing, China). All other chemicals used in this study were of analytical grade.

2.2. Isolation of BDCDs

The BDCDs were extracted using a method described in a previous study, with slight modifications.[24] Briefly, the bread

crust (530 g, wet weight) was first dried in an oven at 60 °C for 2 h, and then the toasted crust edges were collected and ground into a powder (142 g). Next, the bread crust powder was mixed with methanol in a 1 : 20 ratio and sonicated at 40 kHz for 1 h. The mixture was then centrifuged at 5000*g* for 30 min, and the resulting supernatant was concentrated to 1/20 of its original volume using vacuum rotary evaporation. After concentration, the concentrated solution was incubated at 4 °C to allow any insoluble matter to sediment, and then the supernatant was collected for further use. The supernatant was dialyzed in a 3500 Da dialysis bag for 48 h, and the outer dialysis solution was collected for further concentration. To remove small water-soluble molecules, the concentrated outer dialysis solution was dialyzed in a 500 Da dialysis bag for 24 h and then filtered through a 0.22 μm filter. The filtrate was freeze-dried to afford 266 mg of BDCDs (yield was calculated based on the wet weight of bread crust). The obtained BDCDs were then stored in a glass desiccator to prevent moisture absorption for further study.

2.3. Characterization of BDCDs

The characterization of the BDCDs was performed based on the methods described in detail in a previous study.[5] Briefly, the morphology of the BDCDs was characterized using transmission electron microscopy (TEM) (Thermo Fisher Scientific, Waltham, USA). The chemical composition of the BDCDs was characterized using an X-ray photoelectron spectrometer (XPS) (K-Alpha, Thermo Fisher Scientific, Waltham, USA). Their crystalline structure was recorded using an X-ray diffraction (XRD) instrument (D8 Advanced, Bruker, Karlsruhe, Germany). The fluorescence spectra were determined using a spectrofluorometer (F-7000, Hitachi, Tokyo, Japan). The ultraviolet-visible spectra of BDCD suspensions were recorded using a UV-visible spectrophotometer (Multiskan GO, Thermo Fisher Scientific, Waltham, USA).

2.4. BDCD–mucin protein corona formation

BDCD–mucin complexes were prepared according to a method described previously.[25] Briefly, BDCDs and mucin were first mixed together in equal volumes, each at the same concentration, and then the resulting mixture was incubated overnight at 37 °C.

2.5. Scanning electron microscopy

A scanning electron microscope was used to characterize the morphology of the BDCDs, mucin, and BDCD–mucin complexes.[26] These experiments were conducted using a field emission scanning electron microscope (Sigma 360, Zeiss, Oberkochen, Germany). The freeze-dried samples were loaded on conductive tapes and gold-coated prior to SEM observation.

2.6. Zeta potential and particle size analysis

The zeta potentials and particle size distributions of the BDCDs, mucin, and BDCD–mucin complexes were measured using a combined particle electrophoresis/dynamic light scattering instrument (Zetasizer Nano, Malvern Instruments, Malvern, Worcestershire, UK).[26] All the samples were vortex-dispersed evenly before analysis.

2.7. Fourier transform infrared spectroscopy

Freeze-dried BDCDs, mucin, and BDCD–mucin complexes were ground into fine powders. Air was used as a background. The Fourier transform infrared spectra were obtained using a FTIR spectrometer (Nicolet iS50, Thermo Fisher Scientific, Waltham, USA) in the frequency range of 4000 to 400 cm^{-1}.[26]

2.8. Circular dichroism spectroscopy

The circular dichroism spectra of mucin and BDCD–mucin complexes were measured using a CD spectropolarimeter (JASCO J-810, JASCO Corporation, Tokyo, Japan), as previously described.[27] The samples were prepared by mixing 0.5 mg mL^{-1} mucin with concentrations of BDCDs ranging from 0.5 to 2.5 mg mL^{-1}, and then the resulting mixtures were incubated for 24 h. The Beta Structure Selection method was used to calculate the secondary structure of the mucin from the spectra.[28]

2.9. Ultraviolet–visible spectroscopy

The ultraviolet-visible spectra of BDCDs, mucin, and BDCD–mucin complexes were measured using a UV-visible spectrophotometer (Multiskan GO, Thermo Fisher Scientific, Waltham, USA).[29] The concentrations of samples used in this experiment were 0.1 mg mL^{-1}.

2.10. Fluorescence spectroscopy

A spectrofluorometer (F-7000, Hitachi, Tokyo, Japan) and microplate reader (SpectraMax M2, Molecular Devices, Sunnyvale, USA) were used to analyze the interactions between BDCDs and mucin, and between BDCD–mucin complexes and digestive enzymes, respectively. To test the interactions between BDCDs and mucin, an excitation wavelength of 280 nm, an emission wavelength range of 300–500 nm, excitation and emission slit widths of 5 nm, and a scanning rate of 1200 nm min^{-1} were used. To test the interaction between the BDCD–mucin complexes and digestive enzymes, the experiments were conducted by keeping pepsin (2000 U mL^{-1}) and trypsin (100 U mL^{-1}) concentrations constant, while increasing the sample concentrations from 0.5 to 2.5 mg mL^{-1}. The excitation wavelength was set to 280 nm, with an emission wavelength range of 360–500 nm.[30] For the detection of three-dimensional fluorescence spectroscopy, the ranges of excitation wavelength and emission wavelength were 210–390 nm and 250–550 nm, respectively. The test was conducted at room temperature.

2.11. *In vitro* simulated digestion

Simulated digestion was performed as previously described.[31] All experiments were conducted at 37 °C to simulate the conditions in the gastrointestinal tract. The samples subjected to *in vitro* simulated digestion were isolated carbon dots of bread crust (BDCDs), not the bread crust. Four sample groups were prepared: control, BDCDs (10 mg mL^{-1}), mucin (10 mg mL^{-1}),

and BDCD–mucin complexes (10 mg mL^{-1}). Specifically, simulated salivary fluid (15 mL) containing 150 U mL^{-1} α-amylase was mixed with 15 mL of the sample and then incubated for 2 min at pH 7. The concentration of BDCDs in the simulated salivary stage was derived from physiological modeling of oral processing for bread crust, accounting for salivary secretion rates and established extraction yields. Subsequently, the resulting mixture (15 mL) was combined with 15 mL of simulated gastric fluid containing 4000 U mL^{-1} pepsin and incubated for 2 hours at pH 3, with the pH being monitored and adjusted every 30 min to maintain stability.

The mixture (15 mL) was then added to 15 mL of simulated intestinal fluid containing 200 U mL^{-1} trypsin and incubated for 2 hours at pH 7, with the pH monitored and adjusted every 30 min to ensure consistency. After digestion, the digestive enzymes were inactivated by placing the samples in a water bath at 100 °C for 10 min. Simulated digestive fluids without enzymes were used as a negative control.

2.12. Pepsin activity assay

The pepsin activity was quantified as described previously, with slight modifications.[32] Initially, a 0.1 mL aliquot of simulated gastric fluid was added into 0.5 mL of 2% (w/v) bovine hemoglobin solution (pH 2) and incubated at 37 °C for 30 min. Then, the mixture was combined with 1 mL of 5% (w/v) trichloroacetic acid and centrifuged at 12 000*g* for 10 min at 4 °C using a centrifuge (FC5515R, Ohaus, New Jersey, USA). The absorbance of the supernatant at 280 nm was measured.

2.13. Trypsin activity assay

The trypsin activity assay was performed as previously described, with slight modifications.[33] The simulated intestinal fluid was diluted 10-fold and then added to the benzoyl-L-arginine ethyl ester solution (3.1 mL, 0.25 mM). The absorbance of the mixture at 253 nm was then recorded every minute for a duration of 5 min.

2.14. ABTS radical scavenging assay

The ABTS stock solution was prepared by mixing 10 mL of 7 mM ABTS solution with potassium persulfate solution (178 μL, 140 mM) and incubating in the dark overnight.[14] The stock solution was then diluted with dH_2O to achieve an absorbance of 0.7 at 734 nm for further use. The absorbance was measured at 734 nm after incubating the ABTS reaction solution and digestive fluids at room temperature for 1 h.

2.15. Hydroxyl radical scavenging assay

The hydroxyl radical scavenging assay was conducted as previously described, with a slight modification.[14] Equal volumes (0.5 mL each) of digestive fluids, 6 mM $FeSO_4$, 6 mM H_2O_2, and 6 mM salicylic acid–ethanol solution were mixed and incubated at 37 °C for 1 h in the dark. The absorbance was measured at 510 nm. Additionally, the volume of digestive fluid was optimized based on its hydroxyl radical scavenging activity.

2.16. Total reducibility assay

The total reducibility assay was performed as described previously.[14] Briefly, 200 μL of digestive fluids, 200 μL of phosphate buffer solution (200 mM, pH 6.6), and 200 μL of 1% (w/v) potassium ferricyanide were mixed and then incubated at 55 °C for 20 min. Then, 200 μL of 10% (w/v) trichloroacetic acid was added, and the mixture was centrifuged at 1000*g* for 15 min. Next, the supernatant (500 μL) was mixed with 500 μL of dH_2O and 100 μL of 0.17% (w/v) ferric chloride, and incubated at room temperature for 10 min. The absorbance was then measured at 700 nm using a UV-visible spectrophotometer.

2.17. Cell viability assay

Cell viability was assessed using the MTT (3-(4,5-dimethylthiazol-2-yl)-2,5-diphenyltetrazolium bromide) assay.[34] Briefly, Caco-2 cells in a 96-well plate were treated with 200 μL of serum-free medium containing various concentrations (from 6.25 to 1600 μg mL^{-1}) of BDCDs, mucin, and BDCD–mucin complexes for 24 h. After treatment, cells were incubated with MTT for 4 h, and the formazan crystals were dissolved in DMSO. The absorbance at 570 nm was measured using a microplate reader (Thermo Fisher Scientific, Waltham, USA).

2.18. Reactive oxygen species measurement

The measurement of reactive oxygen species (ROS) was carried out as previously described.[34] Caco-2 cells were seeded in a 12-well plate and treated with BDCDs, mucin, and BDCD–mucin complexes at concentrations of 100 and 400 μg mL^{-1} for 24 h. The concentration of BDCDs used in this experiment was calculated based on the mass of bread crust consumed and the total volume of digestive fluids secreted. Then, the cells were incubated with DCFH-DA for 20 min, and images of cells with high ROS levels were captured using a fluorescence microscope (DMi8, Leica, Wetzlar, Germany).

2.19. Statistical analysis

Statistical analysis was conducted by one-way analysis of variance (ANOVA) using OriginPro 2024b software. Results are expressed as mean ± SD. Significance analysis was performed using the Tukey test and Student's *t*-test, with $p < 0.05$ considered statistically significant.

3. Results and discussion

3.1. Characterization of BDCDs

Previous studies have demonstrated that carbon dots are formed during bread baking and exhibit cytotoxicity toward human mesenchymal stem cells *in vitro*.[35] Additionally, it has been reported that nanoparticles can adsorb biomacromolecules from bodily fluids, forming "protein" coronas that play a crucial role in influencing their biological effects.[36] Furthermore, the mucus barrier, which is primarily composed of mucin proteins, serves as the first line of defense in the gastrointestinal tract, protecting the intestinal epithelium from

external damage. Once carbon dots enter the gastrointestinal tract, they therefore interact with mucin in the intestinal mucosa. Therefore, we investigated the impact of mucin corona formation on the gastrointestinal fate of BDCDs.

Initially, the carbon dots were extracted from burnt bread crust and then characterized (Fig. 1A). Fig. 1B shows the photographs of BDCD solutions (1 mg mL^{-1}) when exposed to either visible light or ultraviolet light (365 nm). The BDCD solutions were clear yellowish liquids under visible light but emitted blue fluorescence upon ultraviolet light, indicating that they were fluorescent carbon dots with good water solubility. The morphology of the BDCDs was investigated using transmission electron microscopy (Fig. 1C–E). The regular TEM images showed that the BDCDs consisted of small spheroidal particles with an average diameter of around 5.81 nm, which assembled into clumps of around 100 nm. The high-resolution TEM images showed that the interplane distances within the carbon dots were 0.246 and 0.422 nm. Previous researchers have extracted carbon dots with an average diameter of 2.67 nm from breadcrumbs fried at 180 °C.[37] Thus, the dimensions of the BDCDs extracted from bread crust baked at a similar temperature were on the same order of magnitude as these.

XRD analysis was used to determine the physical state of the BDCDs. The XRD patterns revealed the presence of a single peak at $2\theta = 20.7°$, which suggested that the BDCDs were amorphous (rather than crystalline) (Fig. 1F). According to the XPS analysis, the surface chemical composition of the BDCDs contained C, N, and O constituents, which accounted for 70.9%, 1.5%, and 27.6%, respectively (Fig. 1G and H). Previous studies have reported that nitrogen can increase the quantum yield and enhance the fluorescence of carbon dots,[38,39] which might explain the blue fluorescence of the BDCDs observed in our study. The detailed XPS spectra of C 1s, N 1s, and O 1s were measured to identify the surface functional groups of the BDCDs (Fig. 1I–K). The characteristic peaks at 284.80, 286.39, and 288.29 eV in the C 1s spectra corresponded to C=C/C–C, C–O, and C=O bonds, respectively. In the N 1s spectra, the peaks observed at 399.61, 399.93, and 401.70 eV correspond to pyridinic N, pyrrolic N, and N–H groups, respectively. In the O1s spectra, the peaks observed at 532.12, 532.60, and 534.86 eV correspond to O=C–O, C–O, and O=C–O* functional groups, respectively.[40,41]

Furthermore, the optical properties of the BDCDs were investigated using both fluorescence and UV-visible spectrophotometry. The fluorescence emission spectra of the BDCDs were measured at different excitation wavelengths, revealing a maximum excitation/emission wavelength of 344/437 nm. BDCDs exhibited a quantum yield of 1.03% when excited at 344 nm, along with a decay time of 5.75 ns (Fig. S1†). Additionally, the emission wavelength exhibited a redshift as the excitation wavelength increased, a phenomenon commonly observed in carbon dots (Fig. 1L). Mechanistically, the formation of complex surface states in BDCDs during the bread-baking process may result in this bathochromic emission phenomenon.[5] Moreover, the fluorescence intensity of BDCDs excited by the excitation wavelength of 344 nm decreased with decreasing BDCD concentration (Fig. 1M). However, compared to the fluorescence intensity of BDCDs at 500 μg mL^{-1}, the intensity at 1000 μg mL^{-1} was lower, which could be due to the agglomeration of BDCDs at higher concentrations (as seen in the TEM images), leading to the masking of the fluorophores. The UV-visible spectra of BDCDs had an absorption peak at 276 nm, and the absorbance decreased with decreasing concentration of BDCDs (Fig. 1N). The absorption peak may result from the π–π* conjugation of C=C double bonds in the surface functional groups of BDCDs.[7]

3.2. Interactions between BDCDs and mucin

The interactions between the carbon dots derived from bread crust and mucin were characterized using a variety of analytical methods.

3.2.1. Scanning electron microscopy. To assess whether BDCDs could interact with mucin to form a "protein" corona, mixtures of BDCDs and mucin were prepared and characterized. First, the morphological characteristics of BDCDs, mucin, and the BDCD–mucin complexes were observed by SEM (Fig. 2A). The BDCDs consisted of numerous irregularly shaped particles with dimensions of a few hundred nanometers that were dispersed throughout the samples. Presumably, these particles were the clusters of individual BDCD nanoparticles observed in the TEM images (Fig. 1). Previous researchers have reported that similarly sized clusters of carbon dots are formed when fish (small yellow croaker) is roasted for prolonged durations.[42] The images of the mucin alone suggested that it existed as large clumps with relatively smooth surfaces. The images of the BDCD and mucin mixtures showed that the clusters of carbon dots were embedded within the mucin, indicating the formation of BDCD–mucin complexes.

3.2.2. Zeta potential and particle size analysis. The electrical and size characteristics of the BDCDs, mucin, and BDCD–mucin complexes were measured to provide further insights into the BDCD–mucin complex formation (Fig. 2B and C). All three systems had small to moderate negative surface potentials (−5 to −11 mV). Notably, however, the zeta potential of the BDCD–mucin complexes was much closer to that of the mucin than to that of the BDCDs. This result was consistent with the carbon dot clusters being embedded within the BDCD–mucin complexes, so that the overall surface charge was dominated by the presence of the mucin. Other researchers have also reported that the formation of a protein corona can significantly alter the surface charge of nanoparticles. For instance, after coating with glutenin, the zeta potential of TiO_2 nanoparticles increased from −18.7 mV to +22.6 mV, which was attributed to the fact that the nanoparticles were negatively charged while the proteins were positive charged.[43]

The hydrodynamic diameters of the BDCDs, mucin, and BDCD–mucin complexes were measured by dynamic light scattering. The BDCDs had an average diameter of around 91.28 nm, which was consistent with the dimensions of the particles observed in the TEM images discussed earlier. This

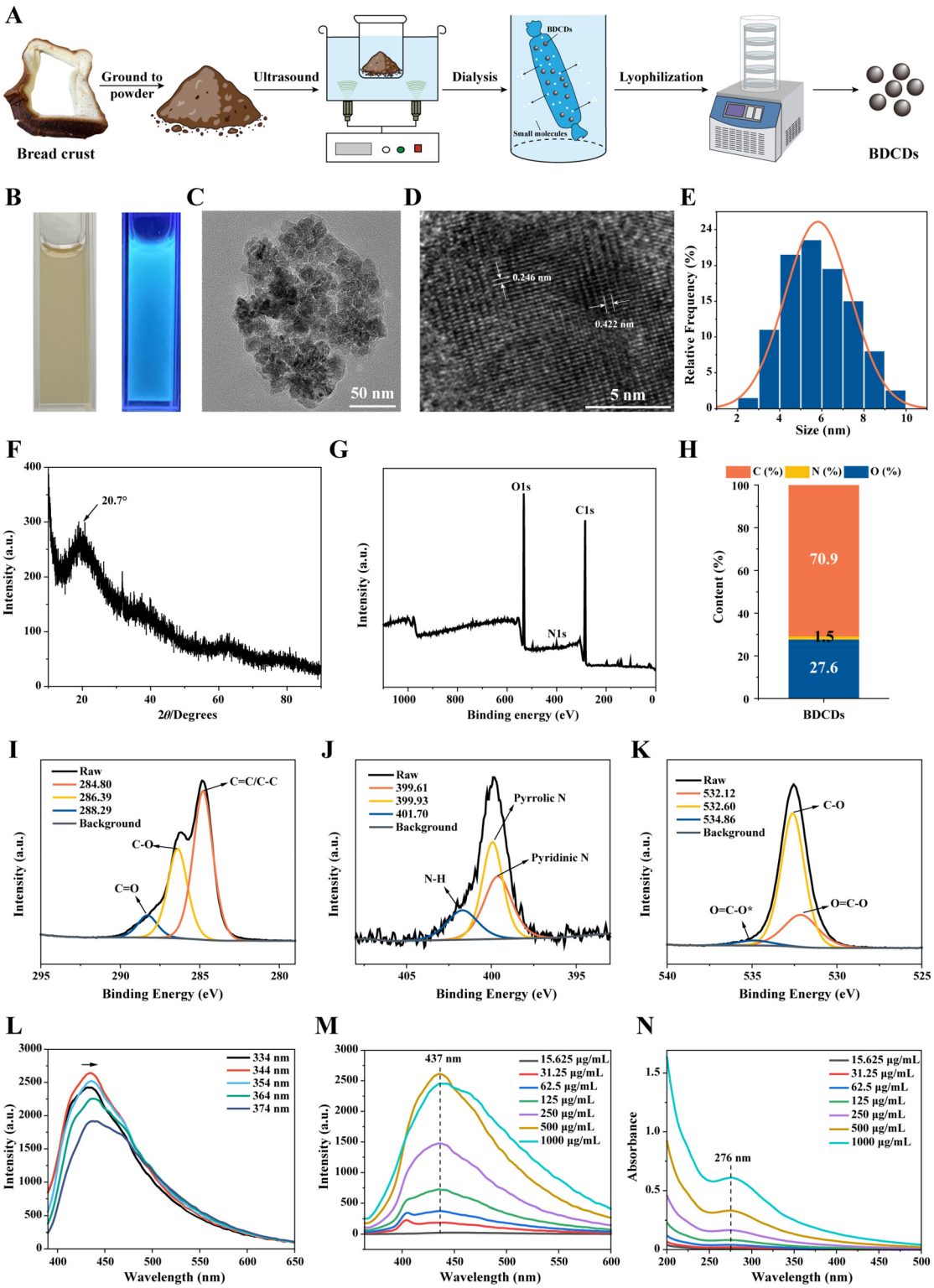

Fig. 1 Characterization of BDCDs extracted from bread crust. (A) The diagram of the extraction of BDCDs. (B) Photographs of the aqueous solution of BDCDs under visible light and UV light (365 nm). (C) TEM image of BDCDs. (D) HR-TEM image of BDCDs. (E) The size distribution histogram of BDCDs. (F) The XRD pattern of BDCDs. (G) The XPS spectrum of BDCDs. (H) The C, N, and O content of BDCDs. (I–K) The detailed XPS spectra of C 1s (I), N 1s (J), and O 1s (K) of BDCDs. (L and M) The fluorescence spectra of BDCDs under different excitation wavelengths (L) and different concentrations (M). (N) The ultraviolet–visible absorption of BDCDs under different concentrations.

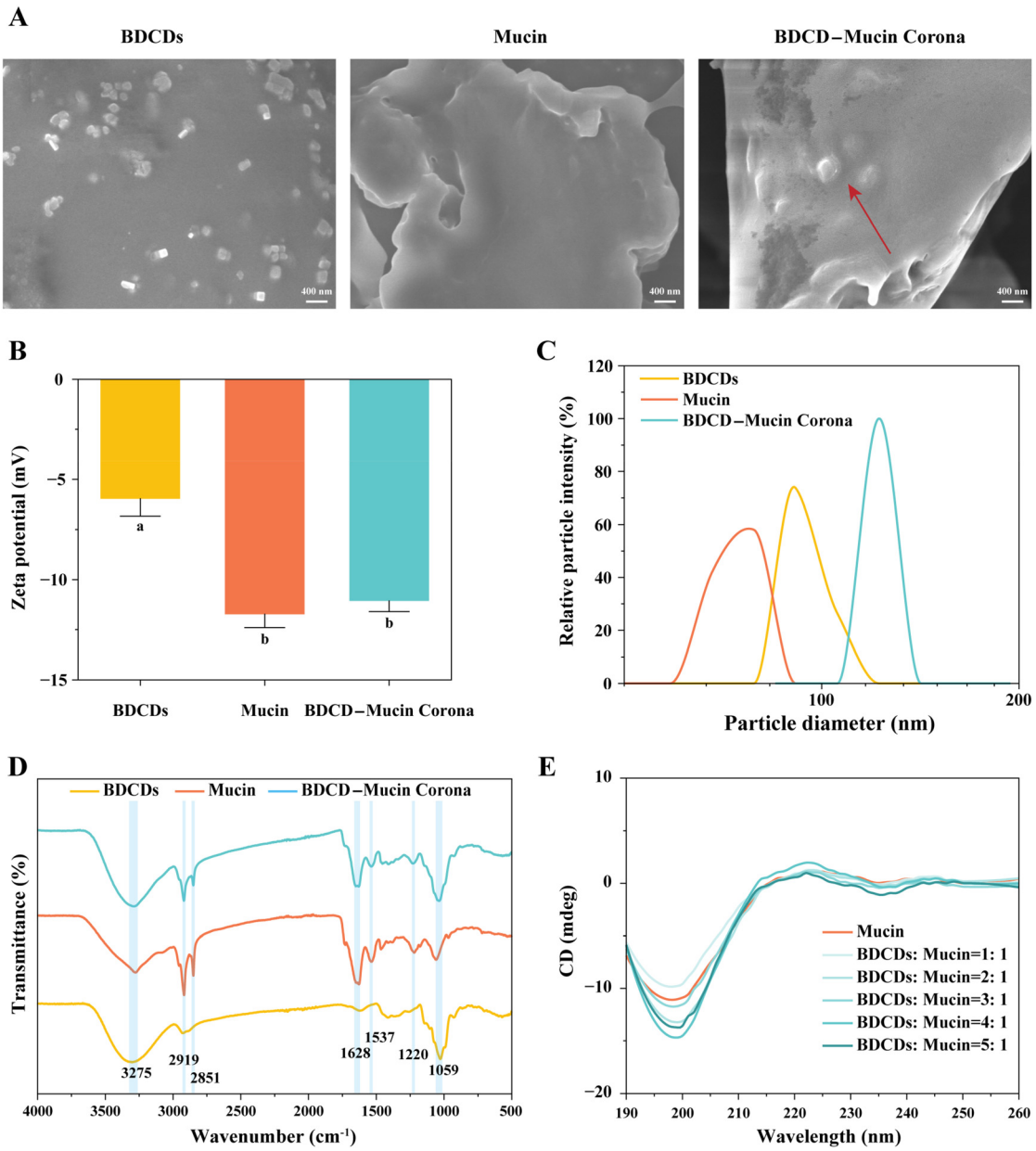

Fig. 2 Characterization of the BDCD–mucin corona. (A) SEM images of BDCDs, mucin, and the BDCD–mucin corona. (B–D) Zeta potential (B), size distribution (C), and FTIR spectra (D) of BDCDs, mucin, and the BDCD–mucin corona. (E) CD spectra of mucin and the BDCD–mucin corona. Bars assigned with different lowercase letters were significantly different (n = 3, p < 0.05, ANOVA, Tukey's test).

size was considerably larger than the size of the individual BDCDs, which again highlights the fact that they tended to exist as clusters in solution. The mucin had an average diameter of around 78.82 nm, which was again consistent with the TEM images, and suggests that the mucin molecules existed as clumps in solution. The average diameter of the BDCD–mucin complexes (122.40 nm) was larger than either the BDCDs or the mucin. This effect may have been because the incorporation of the BDCDs into the clumps of mucin led to an increase in their average size, which was consistent with the SEM images. Other researchers have also reported that the formation of protein–nanoparticle complexes leads to an increase in diameter.[27] Interestingly, however, it has been reported that the formation of a mucin corona can alter the agglomeration state of TiO_2, while only leads to minimal changes in the particle size measured by light scattering.[12] This result suggests that the impact of mucin depends on the nature of the nanoparticles involved.

3.2.3. Fourier transform infrared spectroscopy analysis. To further characterize the interactions between the BDCDs and mucin, changes in the surface functional groups of the BDCDs, mucin, and BDCD–mucin complexes were determined by Fourier Transform Infrared (FTIR) spectroscopy (Fig. 2D). The BDCDs, mucin, and BDCD–mucin complexes all displayed a

similar absorption peak at 3275 cm^{-1}, corresponding to the $-NH_2$ and –OH stretching vibration peak.[22] The peaks found at 2919 and 2851 cm^{-1} were ascribed to the C–H stretching vibrations.[44] The peak at 1628 cm^{-1} corresponded to the stretching vibrations of –COOH, while the peak at 1537 cm^{-1} was ascribed to the C=C group.[30] Meanwhile, the peaks at 1220 and 1059 cm^{-1} corresponded to the C–C stretching vibrations and aromatic alkoxy bonds, respectively.[5] Compared to mucin and the BDCD–mucin complexes, the BDCDs exhibited only small or no peaks at 2919, 2851, 1628, 1537, and 1220 cm^{-1}. After the formation of the BDCD–mucin complexes, a redshift of the $-NH_2$ and –OH stretching vibration peaks of mucin was observed, suggesting hydrogen bonding and hydrophobic interactions between the BDCDs and mucin.[30] Moreover, compared to the mucin group, the peak at 1059 cm^{-1} in the BDCD–mucin complex group exhibited a significant blueshift, suggesting that the BDCDs altered the conformation of mucin. It is worth noting the similarity in the FTIR spectra of mucin and BDCD–mucin complexes, which suggested that mucin dominated the spectra of the complexes. Previous researchers have reported that the presence of a strong amide group peak in the FTIR spectra of nanoparticles was consistent with the adsorption of proteins onto their surfaces.[45]

3.2.4. Circular dichroism spectroscopy analysis. Information about the effects of the BDCDs on the secondary structure of the proteins in the mucin was obtained by circular dichroism (CD) spectroscopy analysis, which is a well-established method for determining the secondary structure of proteins after their interactions with nanoparticles (Fig. 2E).[27] A strong negative band was observed around 200 nm in the CD spectrum of mucin, which indicates a significant amount of β-sheet conformation. Additionally, quantitative analysis of the secondary structure revealed that the β-sheet and random coil contents in mucin were 42.0% and 34.3%, respectively (Table 1).[46] After the formation of the BDCD–mucin complexes, changes in the CD spectra and a redshift in the peak position were observed. Specifically, the mucin peak intensity decreased at a BDCD concentration of 0.5 mg mL^{-1} but then increased when the BDCD concentration exceeded 0.5 mg mL^{-1}. The β-sheet content decreased from 42.0% to 38.2%, the β-turn content increased from 23.7% to 25.7%, and the random coil content increased from 34.3% to 36.7%, indicating an increase in the proportion of disordered regions in mucin after interaction with the BDCDs.[5] Furthermore, as the concentration of BDCDs increased, the secondary structure of mucin underwent various changes, with the random coil content increasing in nearly all BDCD–mucin complex groups, suggesting significant effects of BDCDs on the secondary structure of the mucin.

Table 1 Changes in the secondary structure content of mucin

System	β-Sheet (%)	β-Turn (%)	Random coil (%)
Mucin	42.0	23.7	34.3
BDCDs : mucin = 1 : 1	38.2	25.7	36.1
BDCDs : mucin = 2 : 1	43.7	21.9	34.3
BDCDs : mucin = 3 : 1	39.7	23.2	37.1
BDCDs : mucin = 4 : 1	44.4	23.9	31.7
BDCDs : mucin = 5 : 1	41.8	22.1	36.1

3.2.5. Ultraviolet–visible spectroscopy analysis. To further investigate the interaction between the mucin and BDCDs, as well as the structural changes in mucin, the UV-visible spectra of the BDCD–mucin complexes were measured (Fig. 3A). The pure mucin exhibited one peak at 260 nm corresponding to the π–π transition of aromatic amino acid residues.[23] The intensity of the peak increased and showed a redshift to 261 nm after interacting with the BDCDs, suggesting that the microenvironment of the amino acid residues of mucin was changed. Previous researchers have reported that the interaction between gold nanoparticles and mucin enhances the absorption intensity of mucin at 260 nm in the UV-visible spectrum, suggesting the formation of a protein corona, despite the observed blueshift in the peak.[46]

3.2.6. Fluorescence spectroscopy analysis. Fluorescence spectroscopy is often used to provide information about changes in the structure of proteins. The fluorescence of proteins is mainly generated by tryptophan residues when they are excited at a wavelength of 280 nm. The maximum emission wavelength of tryptophan is considered to be an indicator of its microenvironment: with a maximum emission wavelength greater than 330 nm corresponding to a "polar" microenvironment, and a maximum emission wavelength below 330 nm corresponding to a "non-polar" microenvironment.[47]

The samples were therefore excited using an excitation wavelength of 280 nm and the resulting maximum emission peak around 330 nm was recorded. Compared to mucin alone, there was a red shift of the maximum emission peak of mucin after interacting with BDCDs, which indicated that the presence of the nanoparticles enhanced the polarity of the tryptophan residues in the mucin, suggesting that they altered their microenvironment. Previously, it has been reported that an increase in the polarity of the microenvironment surrounding the aromatic amino acids in the proteins of curcumin–myofibrillar protein complexes led to a red shift in their maximum fluorescence intensity during *in vitro* digestion.[48] Moreover, the fluorescence intensity of the BDCD–mucin complexes was lower than mucin alone, further suggesting the structural changes in the mucin (Fig. 3B). It is important to note that these changes in the microenvironment of the amino acid residues in mucin may disrupt its normal physiological function. For instance, the interaction between black carbon nanoparticles and mucin has been reported to alter the selective permeability of mucin, increasing the translocation of cationic molecules across the mucin barrier.[49]

3.2.7. Three-dimensional fluorescence spectroscopy analysis. Three-dimensional fluorescence contour maps were also used to investigate the spatial conformation of the proteins in the mucin. The fluorescence peak of the BDCDs observed at approximately $\lambda_{ex}/\lambda_{em}$ = 350/440 nm was consistent with our previous fluorescence measurements (Fig. 1F). More importantly, the maximum emission wavelength shifted to longer wavelengths as the excitation wavelength increased, which was

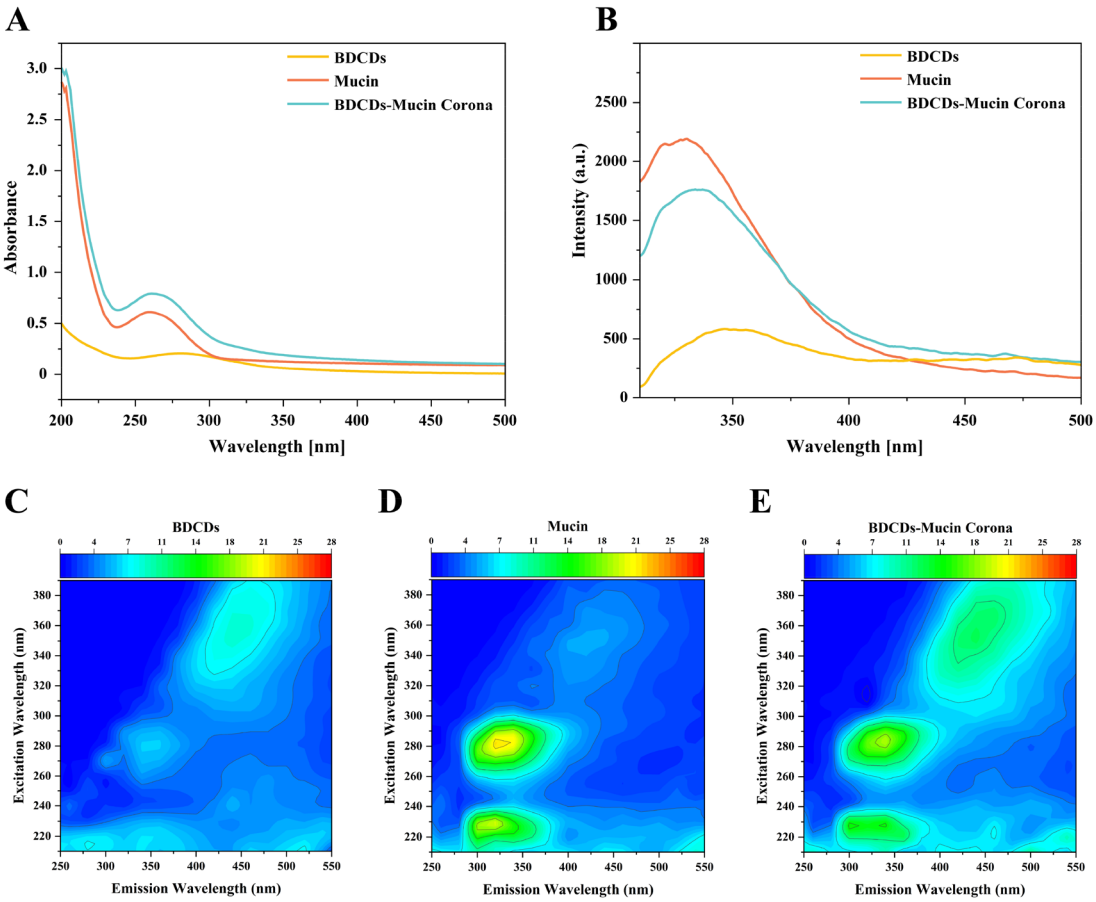

Fig. 3 Optical characteristics of the BDCD–mucin corona. (A) The ultraviolet-visible absorption of BDCDs, mucin, and the BDCD–mucin corona. (B) The fluorescence spectra of BDCDs, mucin, and the BDCD–mucin corona. (C–E) Three-dimensional fluorescence spectra of BDCDs (C), mucin (D), and the BDCD–mucin corona (E).

consistent with the bathochromic emission phenomenon commonly observed in carbon dots (Fig. 3C). For mucin, the fluorescence peak at $\lambda_{ex}/\lambda_{em}$ = 230/320 nm was primarily attributed to the polypeptide backbone, while the peak at $\lambda_{ex}/\lambda_{em}$ = 280/340 nm was attributed to the tryptophan and tyrosine aromatic groups (Fig. 3D).[22]

In the presence of BDCDs, the fluorescence intensity of the mucin at excitation wavelengths of 230 nm and 280 nm decreased, which indicated that both the polypeptide skeleton structure and the tryptophan and tyrosine residues of mucin were involved in its interaction with BDCDs.[50] Moreover, the increased fluorescence intensity observed at an excitation wavelength of 350 nm in the BDCD–mucin complexes also suggests that the BDCDs altered the structure of the proteins in the mucin following their interaction (Fig. 3E). Overall, these results demonstrated that the presence of BDCDs induced a conformational change in the mucin.

3.3. Interactions between BDCD–mucin complexes and digestive enzymes during *in vitro* digestion

In this series of experiments, an *in vitro* digestion model was used to investigate the interactions between the BDCD–mucin complexes and digestive enzymes (Fig. 4A). In general, these *in vitro* simulated digestion models provide a rapid and highly reproducible means of studying the gastrointestinal behavior of foods.[51]

3.3.1. Digestive enzyme activity. Initially, the impact of BDCDs, mucin, and BDCD–mucin complexes on the activity of the digestive enzymes (pepsin and trypsin) was assessed (Fig. 4B and C). The results showed that the activity of pepsin decreased significantly after being treated with BDCDs, while it increased in the mucin group. Interestingly, compared to the BDCD group, the treatment with the BDCD–mucin corona reversed the negative effect of BDCDs on pepsin activity (Fig. 4B). Lei *et al.* have reported that carbon dots with different functional groups can reduce the activity of pepsin to varying degrees, suggesting that the formation of the BDCD–mucin complexes masked the functional groups on the BDCDs that normally interact with pepsin, thereby decreasing its activity in simulated gastric fluids.[20] In general, the physicochemical properties and gastrointestinal behavior of nanoparticles are strongly influenced by the nature of the materials adsorbed to their surfaces, which could explain the differing effects of the BDCDs and BDCD–mucin complexes on enzyme

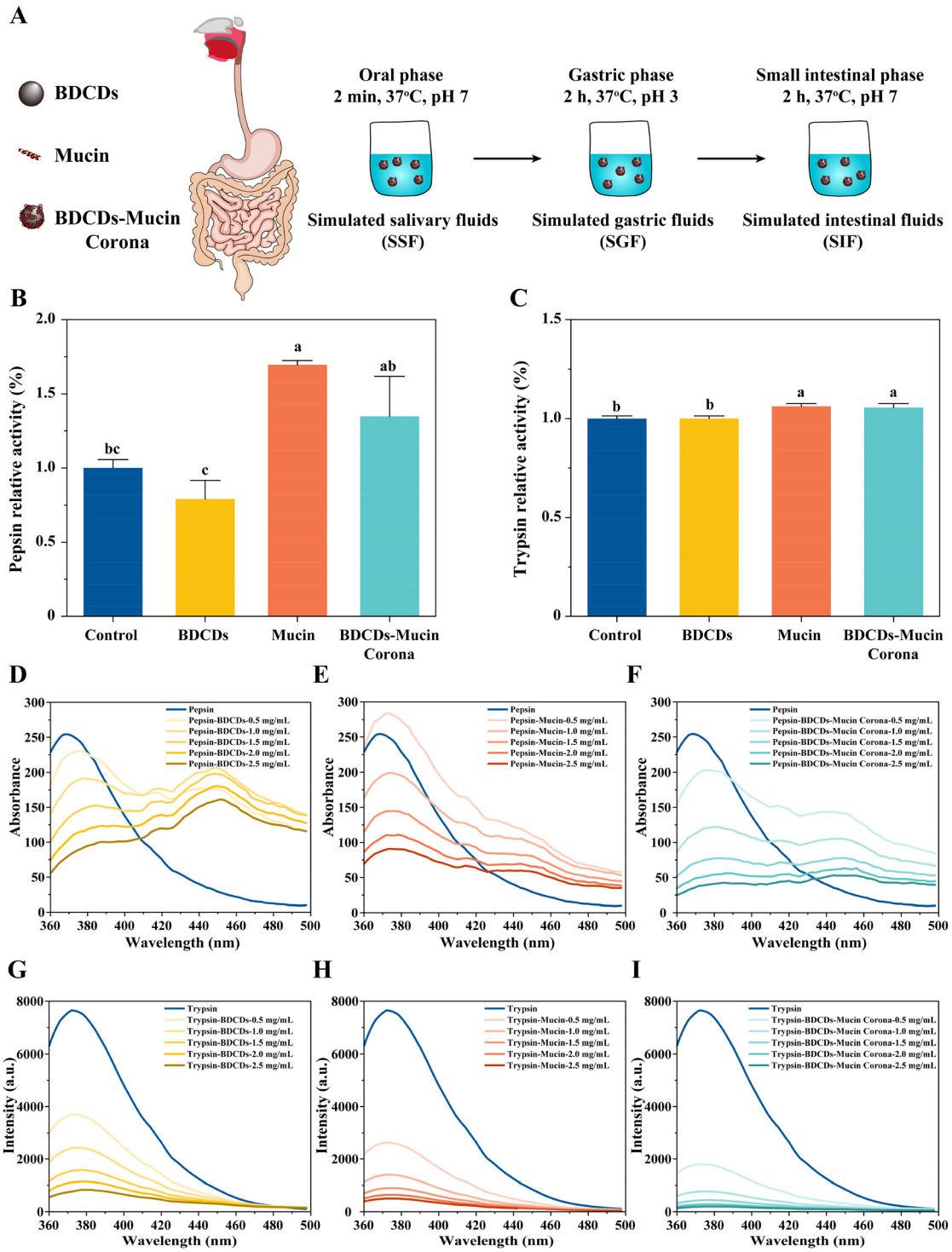

Fig. 4 Effect of BDCDs on digestive enzymes during *in vitro* digestion. (A) The process of *in vitro* simulated digestion. (B and C) The relative activity of pepsin (B) and trypsin (C) during the *in vitro* simulated digestion. (D–F) The fluorescence spectra of pepsin interacting with BDCDs (D), mucin (E), and the BDCD–mucin corona (F). (G–I) The fluorescence spectra of trypsin interacting with BDCDs (G), mucin (H), and the BDCD–mucin corona (I). Bars assigned with different lowercase letters were significantly different ($n = 3$, $p < 0.05$, ANOVA, Tukey's test).

activity.[14] The TEM images discussed earlier showed that the BDCDs were embedded within clumps of mucin (Fig. 1), which may account for the observed decrease in their ability to suppress pepsin activity (Fig. S2†). It has also been reported that carbon dots can interact with pepsin to form a protein corona, which induces a conformational change in the pepsin structure and decreases its activity.[5,52] Interestingly, the BDCDs had much less effect on the activity of trypsin, with no

significant difference compared to the control (Fig. 4C). However, both mucin and the BDCD–mucin complexes caused a slight increase in the activity of the trypsin compared to the control. These results suggest that the impact of the BDCDs and mucin on the activity of digestive enzymes was highly dependent on enzyme type. This effect may have been because of the differences in the interactions of the BDCDs with the enzyme surfaces, as well as due to the differences in the nature of the structural changes in the enzymes, which may have affected the active sites differently.

In summary, these results suggest that mucin may help protect the gastrointestinal digestive function from being impaired by carbon dots in foods.

3.3.2. Fluorescence spectroscopy analysis of digestive enzymes. Further insights into the impact of mucin on carbon dot–mucin interactions were obtained by measuring the fluorescence spectra of the digestive enzymes after interacting with BDCDs, mucin, and BDCD–mucin complexes. The fluorescence intensity of the pepsin gradually decreased as the concentrations of BDCDs and BDCD–mucin complexes increased (Fig. 4D–F). In contrast, the fluorescence intensity of pepsin increased after interaction with 0.5 μg mL^{-1} mucin but decreased progressively as the mucin concentration was increased further. These results indicated that the interactions between our samples and pepsin induced structural changes in the pepsin, although they had different effects on its activity. Moreover, the peak of pepsin showed a redshift, suggesting that the polarity of its amino acid residues increased after interacting with BDCDs, mucin, and the BDCD–mucin complexes. Li *et al.* observed a significant decrease in the fluorescence emission intensity of digestive enzymes with increasing nanoparticle concentration, which suggested their interaction and subsequent fluorescence quenching.[53] Interestingly, the redshift of pepsin was most pronounced in the BDCD–mucin complex group, followed by the BDCD and mucin groups. In addition, the fluorescence spectra of the BDCDs and BDCD–mucin complex groups had two peaks, which were attributed to the presence of the BDCDs. Notably, our previous fluorescence spectroscopy results of BDCDs, mucin, and BDCD–mucin complexes showed no fluorescence peak at 450 nm when excited at 280 nm (Fig. 3B). This suggested that the interaction between BDCDs and pepsin resulted in the emergence of a new fluorescence peak upon excitation at 280 nm. A previous study reported that cobalt oxyhydroxide catalytically oxidized *o*-phenylenediamine, resulting in the formation of a new fluorescence peak at 556 nm and a decrease in the fluorescence intensity of silicon nanoparticles at 443 nm within a fluorescent nanoprobe, thereby generating a double-peak fluorescence spectrum.[54] However, compared to the BDCD group, the interaction between the BDCD–mucin corona and pepsin reduced the intensity of the fluorescence peak at 450 nm, which may explain the restored activity of pepsin in the BDCD–mucin complex group. A previous report found that a different amino-modified starch nanoparticle did not affect pepsin activity, despite significant interaction with pepsin.[55]

The fluorescence intensity of trypsin displayed a trend similar to that of pepsin after interacting with BDCDs, mucin, and the BDCD–mucin complexes (Fig. 4G–I). However, the key difference was the absence of a fluorescence peak at 450 nm. These results suggest that the presence of our samples altered the structure of trypsin, although they had little effect on its activity. Wang *et al.* reported that epigallocatechin gallate-resistant starch nanoparticles altered the conformation and microenvironment of trypsin, while leaving its activity unaffected.[30] Again, the above results suggest that BDCDs have little effect on the active site of trypsin, while the presence of mucin or BDCD–mucin complexes may even activate trypsin. Furthermore, the redshift of the trypsin peak was slightly smaller than that of pepsin when treated with BDCDs, mucin, and the BDCD–mucin complexes, which may correspond to the smaller changes in trypsin activity observed for these treatments.

The quenching mechanisms of pepsin and trypsin were investigated using the Stern–Volmer equation (Fig. S3†). According to the F_0/F curve, a linear correlation was observed with BDCDs, mucin, and BDCD–mucin complexes at concentrations ranging from 0.5 to 2.5 μg mL^{-1}, which suggests that the Stern–Volmer equation was appropriate for interpreting the data. Furthermore, the slight upward curvature observed in the F_0/F curve suggests the coexistence of static and dynamic quenching. These energy results suggest that BDCDs, mucin, and BDCD–mucin complexes could interact with pepsin and trypsin to form non-fluorescent complexes, accompanied by a charge or transfer between them.[56–58] Compared to BDCDs alone, the BDCD–mucin complexes exhibited a weaker linear relationship with pepsin and trypsin, suggesting that reduced non-fluorescent complexes formed between the complexes and these enzymes.

3.4. Changes in the antioxidant activity of BDCD–mucin complexes induced by *in vitro* digestion

It has been reported that free radicals are generated during aerobic metabolism and can influence the physiological functions and metabolism of the human body.[59] Studies have shown that mucins can protect DNA from hydroxyl radical damage and that sialic acid in mucin is an essential component of its antioxidant activity.[60] Therefore, the antioxidant activity of BDCDs, mucin, and BDCD–mucin complexes during *in vitro* simulated digestion was measured using three assays: the ABTS radical scavenging, hydroxyl radical scavenging, and total reducibility assays. The results of the ABTS radical scavenging assay indicated that the formation of the BDCD–mucin complexes increased the ability of the BDCDs to scavenge ABTS radicals during the simulated salivary and intestinal stages (Fig. 5A–D). Notably, the mucin itself had a relatively low ABTS radical scavenging ability during the simulated gastric stage. After exposure to simulated gastric conditions, the ABTS radical scavenging ability of the BDCD–mucin complexes was lower than that of the BDCDs, which may be because the carbon dots were trapped inside mucin clumps. Furthermore, the ABTS radical scavenging ability of BDCDs,

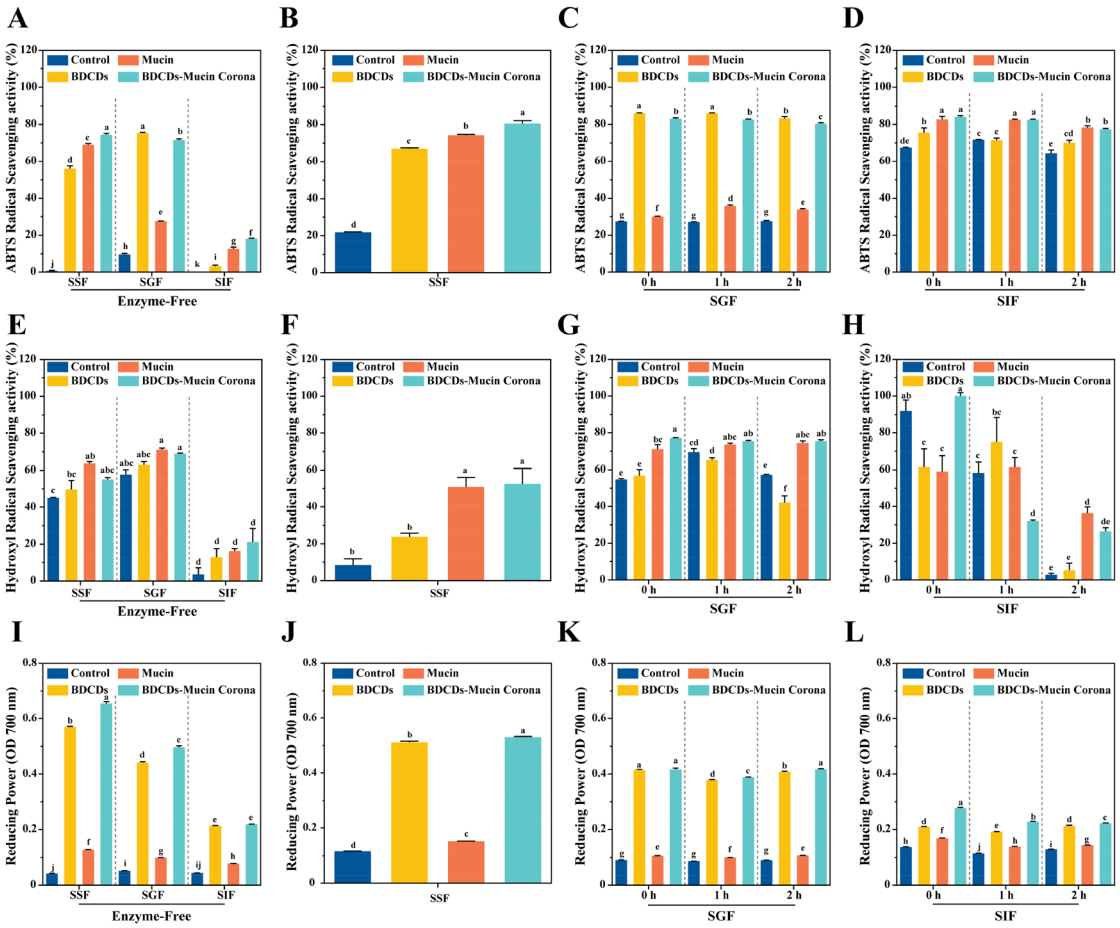

Fig. 5 The antioxidant activity of BDCDs, mucin, and the BDCD–mucin corona during *in vitro* digestion. (A–D) ABTS radical scavenging ability of BDCDs, mucin, and the BDCD–mucin corona in simulated salivary fluid, simulated gastric fluid, and simulated intestinal fluid (E and F) The OH^- radical scavenging ability of BDCDs, mucin, and the BDCD–mucin corona in simulated salivary fluid, simulated gastric fluid, and simulated intestinal fluid. (I–L) The total reducibility of BDCDs, mucin, and the BDCD–mucin corona in simulated salivary fluid, simulated gastric fluid, and simulated intestinal fluid. The digestive juice without digestive enzymes was used as a control. Bars assigned with different lowercase letters were significantly different ($n = 3$, $p < 0.05$, ANOVA, Tukey's test).

mucin, and BDCD–mucin complexes remained stable, with only a slight decline at each stage of digestion, indicating their relative resistance to digestive processes

Typically, an increase in the antioxidant activity of proteins during simulated digestion occurs due to the generation of antioxidant peptides after hydrolysis by proteases. Previous studies have shown that mucin is relatively resistant to digestion by digestive enzymes in the gastrointestinal tract, which is consistent with the stable ABTS radical scavenging activity of mucin and the BDCD–mucin complexes when exposed to different digestion regions.[61]

Interestingly, the results of the hydroxyl radical scavenging assay were similar to those of the ABTS radical scavenging assay (Fig. 5E–H). The hydroxyl radical scavenging ability of mucin remained high during the simulated gastric phase. Moreover, the hydroxyl radical scavenging ability of the BDCDs significantly decreased during the simulated gastric and intestinal phases as digestion progressed, suggesting that digestive enzymes may interact with BDCDs to form protein coronas, thereby masking the reducing groups on their surfaces.[5] However, in simulated gastric fluids, the hydroxyl radical scavenging ability of the BDCD–mucin complexes remained unchanged, suggesting that the formation of the mucin protein corona prevented further interaction between the BDCDs and digestive enzymes. It should be noted that the hydroxyl radical scavenging activity of the BDCD–mucin complexes decreased significantly during the simulated intestinal phase, although it remained higher than that of the BDCDs at the end of digestion. One possible explanation is that the structure changes of the BDCD–mucin complexes during the simulated intestinal phase resulted in masking of the reducing groups on their surfaces.

In the total reducibility assay, mucin exhibited a low reducing ability throughout the *in vitro* simulated digestion, whereas the BDCDs retained a relatively high reducing ability. As shown in Fig. 5J–L, it is clear that the formation of the BDCD–mucin complexes enhanced the reducing ability of the BDCDs during simulated digestion. Previous studies have

reported that the formation of a whey protein corona around TiO_2 nanoparticles enhanced their antioxidant properties. However, TiO_2 nanoparticles may also reduce the antioxidant activity of whey by adsorbing some of the proteins and peptides onto their surfaces.[14] Furthermore, the reducing ability of the BDCDs, mucin, and BDCD–mucin complexes decreased slightly after each stage of digestion, which was consistent with the results of the ABTS radical scavenging assay. These results suggest that the BDCD–mucin complexes remain relatively stable in the gastrointestinal tract. It should be noted, however, that compared to the antioxidant activity of simulated digestive fluid without digestive enzymes, the presence of digestive enzymes enhanced the antioxidant activity of the digestive fluids (Fig. 5).

Based on the antioxidant activity results, it can be speculated that the BDCD–mucin complexes remained relatively stable during simulated digestion, which may allow them to play a role in the colon.

Interestingly, although the antioxidant activity of the BDCDs, mucin, and BDCD–mucin complexes exhibited some fluctuations during *in vitro* simulated digestion, the BDCD–mucin complexes demonstrated higher antioxidant activity than the BDCDs but lower than the mucin at the end of the digestion process, particularly for the ABTS and hydroxyl radical scavenging capacities. A plausible explanation for this effect is that the reductive peptides of mucin were adsorbed onto the surface of BDCDs, resulting in a reduced radical scavenging activity compared to that of free mucin.[14] Additionally, the presence of BDCDs may modulate the diversity and abundance of peptides generated during simulated digestion.[62] In comparison with BDCDs alone, the enhanced antioxidant activity of the BDCD–mucin complexes could be attributed to the surface chemistry modification of the BDCDs by mucin, which may further shield BDCDs from interactions with other gastrointestinal components, such as digestive enzymes, thereby maintaining a relatively high antioxidant activity.

Additional information about the stability of the BDCD–mucin complexes during the digestion process was obtained by measuring changes in their fluorescence and UV-visible absorption spectra after being exposed to different pH conditions, which were designed to simulate the gastrointestinal environment (Fig. S4†). These results showed that there were some modest changes in the fluorescence and UV-visible absorption spectra after exposure of the BDCD–mucin complexes to simulated gastrointestinal conditions, which suggests that there were some alterations in protein conformation and/or the aggregation state of the complexes when exposed to different digestion conditions. These alterations may account for the changes in the antioxidant properties of the complexes in different gastrointestinal regions discussed earlier.

3.5. Biological effects of the BDCD–mucin complexes on intestinal epithelial cells

Finally, the potential biological effects of the carbon dot–mucin complexes were determined by measuring their impact on the viability and oxidation state of model intestinal epithelial cells.

3.5.1. Cell viability. Studies have shown that carbon dots extracted from foods inhibit cell growth, an effect that can be mitigated by the formation of a protein corona.[25] Therefore, an MTT assay was conducted to assess the viability of intestinal epithelial cells treated with BDCDs and BDCD–mucin complexes. Caco-2 cells were used as an *in vitro* model of the intestinal epithelium in our study because they mimic many of the features of human gastrointestinal cells.[63] Our results demonstrated that BDCDs reduced Caco-2 cell viability in a concentration-dependent manner, indicating their detrimental effects on intestinal epithelial cells (Fig. 6A). Previously, it has been reported that carbon dots extracted from roasted chicken breasts (300 °C) decrease the cell viability of Caco-2 cells by approximately 60% when applied at a concentration of 1 mg mL^{-1} for 3 hours.[64] In contrast, BDCDs exhibited a relatively lower level of cytotoxicity, with about a 20% reduction in cell viability at concentrations ranging from 400 to 1600 μg mL^{-1}. These findings suggest that carbon dots generated in foods at higher temperatures may pose greater risks to human health. Interestingly, the presence of mucin did not decrease the cell viability of the Caco-2 at concentrations lower than 1600 μg mL^{-1}, and even increased cell viability at 400 μg mL^{-1} (Fig. 6B). It is worth noting that the formation of a mucin corona enhanced the viability of Caco-2 cells compared to the BDCDs group, particularly at concentrations ranging from 50 to 400 μg mL^{-1}, suggesting a toxicity alleviation effect of the mucin corona (Fig. 6C and D). Our previous studies also demonstrated that the formation of a glutenin protein corona protected Caco-2 cells from injury induced by TiO_2 nanoparticles, which is consistent with the findings of the present study.[34] However, it has been reported that two-dimensional graphene oxide nanosheets with low serum protein binding exhibit lower cell viability in J774 cells compared to graphene oxide nanosheets alone.[65] All these findings indicate that the effect of a protein corona on cell viability depends on the proteins present in the corona layer, the nature of the nanomaterials used, and the origin of the protein–nanomaterial interactions.[16]

3.5.2. ROS level. As oxidative damage is a key toxic effect of nanoparticles, we investigated the impact of mucin corona formation on the ROS levels induced by BDCDs in Caco-2 cells.[25] Our results showed that the BDCD–mucin complexes significantly increased the viability of Caco-2 cells at concentrations ranging from 50 to 400 μg mL^{-1}. Therefore, we selected concentrations of 100 and 400 μg mL^{-1} for the ROS study. As shown in Fig. 6E, compared to the control group, treatment with BDCDs increased the ROS levels in a dose-dependent manner. Additionally, mucin slightly increased the ROS levels in the Caco-2 cells, but no further increase was observed with higher concentrations of mucin, which was consistent with the results of the MTT assay. As expected, the BDCD–mucin complexes significantly decreased the ROS levels in the Caco-2 cells, suggesting that the formation of a mucin corona could scavenge ROS generation induced by BDCDs. A previous study

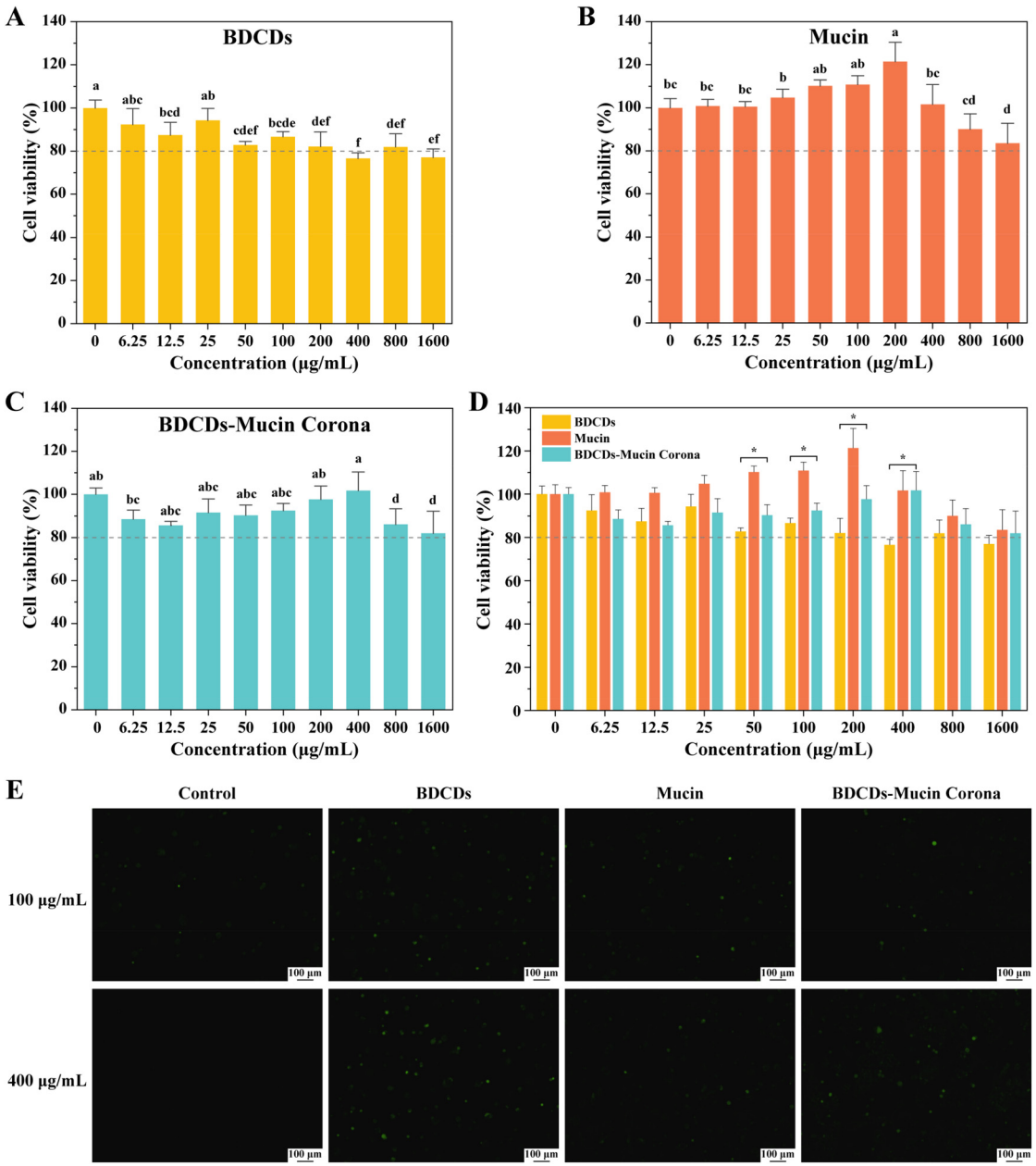

Fig. 6 Biological effects of BDCDs, mucin, and the BDCD–mucin corona on Caco-2 cells. (A–D) Cell viability of Caco-2 cells treated with BDCDs, mucin, and the BDCD–mucin corona for 24 h. (E) ROS levels detected in Caco-2 cells after incubation with BDCDs, mucin, and the BDCD–mucin corona for 24 h. *$p < 0.05$ *vs.* the BDCD group ($n = 6$, Student's *t*-test). Bars assigned with different lowercase letters were significantly different ($n = 6$, $p < 0.05$, ANOVA, Tukey's test).

reported that a mucin corona around polystyrene–benzopyrene nanoparticles reduced ROS production in A549 cells by altering the cellular uptake and intracellular trafficking of the nanoparticles.[66] This suggests that the decreased ROS levels in the Caco-2 cells may be due to changes in the cellular uptake and transport of the BDCDs following the formation of BDCD–mucin complexes. Previous researchers have also reported that a mucin protein corona can modulate the uptake and translocation of nanoparticles in and across intestinal epithelial cells.[13,67] However, the mechanism by which mucin coronas alleviate BDCD-induced cellular injury and elevated ROS levels still remains unclear.

4. Conclusion

In summary, this study characterized the carbon dots isolated from bread crust and then investigated their interactions with mucin. The bread-derived carbon dots (BDCDs) were found to interact with mucin and form BDCD–mucin complexes, where

clusters of carbon dots were embedded within mucin clumps. The formation of these complexes led to changes in zeta potential and particle size of the BDCDs, as well as alterations in the secondary structure of the mucin. *In vitro* simulated digestion showed that BDCDs reduced pepsin activity by altering its conformation, as evidenced by changes in the fluorescence spectrum. Furthermore, the presence of mucin reduced the ability of the BDCDs to inactivate pepsin, and actually increased the activity of trypsin. The antioxidant activity of BDCDs during simulated digestion was found to be enhanced by the formation of the carbon dot–mucin clusters. Additionally, compared to the BDCDs, the BDCD–mucin complexes enhanced the viability of Caco-2 cells by reducing cellular ROS levels. Our results highlight the impact of mucin on the gastrointestinal behavior of food-derived carbon dots, which may be important in understanding their potential adverse effects on the healthiness of foods.

Author contributions

Mi Shichao: writing – original draft, methodology, formal analysis, investigation, and data curation. Liu Zimo: methodology, formal analysis, and data curation. Wang Mingcheng: methodology and formal analysis. David Julian McClements: formal analysis and review & editing. Cao Chongjiang: conceptualization and validation. Xu Xiao: formal analysis, visualization, supervision, validation, and review & editing. Yuan Biao: funding acquisition, conceptualization, supervision, review & editing, and project administration

Data availability

The data will be made available from the corresponding author upon reasonable request.

Conflicts of interest

There are no conflicts of interest to declare.

Acknowledgements

This work was supported by the National Natural Science Foundation of China (32472355, 31901699 and 32302040), the Fundamental Research Funds for the Central Universities (2632021ZD01 and 2632024HL03), the China Postdoctoral Science Foundation (2020T130138ZX), the Jiangsu Planned Projects for Postdoctoral Research Funds and the National Innovation and Entrepreneurship Training Program for Undergraduate.

References

1 D. H. H. Nguyen, H. El-Ramady and J. Prokisch, Food safety aspects of carbon dots: a review, *Environ. Chem. Lett.*, 2025, **23**, 337–360.
2 H. E. Emam, Carbon quantum dots derived from polysaccharides: Chemistry and potential applications, *Carbohydr. Polym.*, 2024, **324**, 121503.
3 H. Wang, W. Su and M. Tan, Endogenous fluorescence carbon dots derived from food items, *Innovation*, 2020, **1**, 100009.
4 B. Zhang, X. Fan, H. Du, M. Zhao, Z. Zhang, R. Zhu, B. He, Y. Zhang, X. Li, J. Li and N. Gu, Foodborne carbon dot exposure induces insulin resistance through gut microbiota dysbiosis and damaged intestinal mucus layer, *ACS Nano*, 2023, **17**, 6081–6094.
5 X. Song, Y. Song, Z. Guo and M. Tan, Influence of protein coronas between carbon nanoparticles extracted from roasted chicken and pepsin on the digestion of soy protein isolate, *Food Chem.*, 2022, **385**, 132714.
6 H. B. Ahmed, M. El-Shahat, A. K. Allayeh and H. E. Emam, Maillard reaction for nucleation of polymer quantum dots from chitosan-glucose conjugate: Antagonistic for cancer and viral diseases, *Int. J. Biol. Macromol.*, 2023, **224**, 858–870.
7 R. Liu, K. Liu and M. Tan, Nanocorona formation between foodborne nanoparticles extracted from roast squid and human serum albumin, *J. Agric. Food Chem.*, 2019, **67**, 10470–10480.
8 R. Liu, K. Liu, G. Cui and M. Tan, Change of cell toxicity of food-borne nanoparticles after forming protein coronas with human serum albumin, *J. Agric. Food Chem.*, 2022, **70**, 1261–1271.
9 C. Song, Z. Chai, S. Chen, H. Zhang, X. Zhang and Y. Zhou, Intestinal mucus components and secretion mechanisms: what we do and do not know, *Exp. Mol. Med.*, 2023, **55**, 681–691.
10 N. Reznik, A. D. Gallo, K. W. Rush, G. Javitt, Y. Fridmann-Sirkis, T. Ilani, N. A. Nairner, S. Fishilevich, D. Gokhman, K. N. Chacón, K. J. Franz and D. Fass, Intestinal mucin is a chaperone of multivalent copper, *Cell*, 2022, **185**, 4206–4215.
11 X. Rui, K. Fu, H. Wang, T. Pan and W. Wang, Formation mechanisms of protein coronas on food-related nanoparticles: their impact on digestive system and bioactive compound delivery, *Foods*, 2025, **14**, 512.
12 H. Zhou, J. K. Pandya, Y. Tan, J. Liu, S. Peng, J. L. Muriel Mundo, L. He, H. Xiao and D. J. McClements, Role of mucin in behavior of food-grade tio2 nanoparticles under simulated oral conditions, *J. Agric. Food Chem.*, 2019, **67**, 5882–5890.
13 D. Yang, Y. Feng, Y. Yuan, L. Zhang, Y. Zhou, A. C. Midgley, Y. Wang, N. Liu, G. Li, X. Yao and D. Liu, Protein coronas derived from mucus act as both spear and shield to regulate transferrin functionalized nanoparticle transcellular transport in enterocytes, *ACS Nano*, 2024, **18**, 7455–7472.

14 H. Shan, Y. Guo, J. Li, Z. Liu, S. Chen, B. Dashnyam, D. J. McClements, C. Cao, X. Xu and B. Yuan, Impact of whey protein corona formation around tio2 nanoparticles on their physiochemical properties and gastrointestinal fate, *J. Agric. Food Chem.*, 2024, **72**, 4958–4976.

15 G. Lee, Y.-J. Jhang, Y.-T. Jhang, Y.-C. Chang, H.-W. Chang, C.-Y. Chuang, Y.-K. Chuang, C.-W. Lin and I. L. Hsiao, Artificial digestion represents the worst-case scenario for studying nanoplastic fate in gastrointestinal tract, *J. Hazard. Mater.*, 2025, **485**, 136809.

16 R. Liu, D. Yu, A. M. Abd El-Aty and M. Tan, Protein corona of food nanoparticles: Implications for biological responses and future research directions, *Trends Food Sci. Technol.*, 2023, **141**, 104179.

17 Y. Wang, Y. L. Mo, Y. W. Sun, J. Li, Y. An, N. P. Feng and Y. Liu, Intestinal nanoparticle delivery and cellular response: a review of the bidirectional nanoparticle-cell interplay in mucosa based on physiochemical properties, *J. Nanobiotechnol.*, 2024, **22**, 669.

18 J. Wang, Z. Zhang, Z. Zhang, Z. Zou, Y. Zhuo, C. Liu, D. Nie, Y. Gan and M. Yu, Enhanced gut-to-liver oral drug delivery via ligand-modified nanoparticles by attenuating protein corona adsorption, *ACS Nano*, 2024, **18**, 35310–35324.

19 Q. Peng, Y. Ma, Z. Wang and J. Wang, Inhibition mechanism of different structural polyphenols against α-amylase studied by solid-state NMR and molecular docking, *Int. J. Biol. Macromol.*, 2024, **275**, 133757.

20 C. Lei, M. Tao, L. Xu, L. Yue, X. Cao, B. Cheng, C. Wang and Z. Wang, Different functional groups of carbon dots influence the formation of protein crowns and pepsin characteristic *in vitro* digestion, *Food Chem.*, 2024, **440**, 138224.

21 Y. Chen, Q. Liu, H. Yu, Y. Guo, Y. Cheng, H. Qian, Y. Xie and W. Yao, Protein corona formed on the TiO2 nanoparticles promotes the hydrolysis of collagen in simulated gastrointestinal fluids, *Food Biosci.*, 2023, **53**, 102786.

22 Y.-R. Wu, Q. Zhou, J. Li, W. Wang, Y.-B. Zhou and K. Liu, The formation of protein coronas and its effect on the quercetin-edible dock protein nanoparticles, *Food Hydrocolloids*, 2024, **157**, 110432.

23 Y. Wang, L. Zhou, Y. Sun, H. Mu, X. Li, Y. Wang and Q. Sun, Formation of protein corona on interaction of pepsin with chitin nanowhiskers in simulated gastric fluid, *Food Chem.*, 2022, **383**, 132393.

24 Q. Huang, L. Yan, H. Wei, X. Ye, W. Wang, C. Yang, X.-P. Yan and Y. Zhang, Extraction, characterization and toxicity evaluation of fluorescent carbon nanoparticles in bamboo charcoal peanut, *J. Food Compos. Anal.*, 2023, **121**, 105357.

25 K. Liu, Y. Song and M. Tan, Toxicity alleviation of carbon dots from roast beef after the formation of protein coronas with human serum albumin, *J. Agric. Food Chem.*, 2020, **68**, 9789–9795.

26 Q. Zhao, H. Shan, Y. Li, B. Jiang, X. Xu, D. Julian McClements, C. Cao and B. Yuan, Investigation of the interactions between food plant carbohydrates and titanium dioxide nanoparticles, *Food Res. Int.*, 2022, **159**, 111574.

27 H. Shan, Q. Zhao, Y. Guo, M. Gao, X. Xu, D. J. McClements, C. Cao and B. Yuan, Impact of pH on the formation and properties of whey protein coronas around TiO2 nanoparticles, *J. Agric. Food Chem.*, 2023, **71**, 5756–5769.

28 A. Micsonai, É. Moussong, F. Wien, E. Boros, H. Vadászi, N. Murvai, Y.-H. Lee, T. Molnár, M. Réfrégiers, Y. Goto, Á. Tantos and J. Kardos, BeStSel: webserver for secondary structure and fold prediction for protein CD spectroscopy, *Nucleic Acids Res.*, 2022, **50**, W90–W98.

29 B. Jiang, Q. Zhao, H. Shan, Y. Guo, X. Xu, D. J. McClements, C. Cao and B. Yuan, Impact of heat treatment on the structure and properties of the plant protein corona formed around TiO2 nanoparticles, *J. Agric. Food Chem.*, 2022, **70**, 6540–6551.

30 S. Wang, Z. Duan, L. Zheng, Y. Yang, X. Zheng, D. Xiao, B. Ai, M. Wang and Z. Sheng, Digestive enzyme corona formed in simulated gastrointestinal tract and its impact on EGCG release from banana resistant starch nanoparticles, *Food Hydrocolloids*, 2024, **146**, 109267.

31 H. Yang, P. Wilde, R. J. Wang, Q. Meng, H. Y. Shi, H. Yu, Z. J. Zhou, J. Z. Han and W. L. Liu, Effect of complexation with different molecular weights of oat β-glucan and sea buckthorn flavonoid on the digestion of rice flour, *J. Agric. Food Chem.*, 2024, **72**, 23567–23579.

32 J. Zhang, Q. Li, X. Jiang, X. Li, P. Dong, J. Li, M. Komiyama and X. Liang, Effect of sulfated polysaccharides on the digestion of DNA by pepsin under simulated gastric juice *in vitro*, *Food Funct.*, 2020, **11**, 1790–1797.

33 M. Sun, Z. Cai, C. Li, Y. Hao, X. Xu, K. Qian, H. Li, Y. Guo, A. Liang, L. Han, H. Shang, W. Jia, Y. Cao, C. Wang, C. Ma, J. C. White and B. Xing, Nanoscale ZnO improves the amino acids and lipids in tomato fruits and the subsequent assimilation in a simulated human gastrointestinal tract model, *ACS Nano*, 2023, **17**, 19938–19951.

34 S. Mi, M. Shen, Z. Liu, Y. Yu, H. Shan, J. Cao, D. J. McClements, C. Cao, X. Xu and B. Yuan, A glutenin protein corona ameliorated TiO2 nanoparticle-induced gut barrier dysfunction and altered the gut microbiota composition, *Food Funct.*, 2024, **15**, 12101–12117.

35 A. M. Al-Hadi, V. S. Periasamy, J. Athinarayanan, A. S. Al-Khalifa and A. A. Alshatwi, Extraction of ultrafine carbon nanoparticles from samooli Bread and evaluation of their *in vitro* cytotoxicity in human mesenchymal stem cells, *Process Biochem.*, 2017, **52**, 250–258.

36 H. Tang, Y. Zhang, T. Yang, C. Wang, Y. Zhu, L. Qiu, J. Liu, Y. Song, L. Zhou, J. Zhang, Y. K. Wong, Y. Liu, C. Xu, H. Wang and J. Wang, Cholesterol modulates the physiological response to nanoparticles by changing the composition of protein corona, *Nat. Nanotechnol.*, 2023, **18**, 1067–1077.

37 J. Yin, K. Liu, S. Yuan, Y. Guo, H. Yu, Y. Cheng, Y. Xie, H. Qian and W. Yao, Carbon dots in breadcrumbs: Effect of

frying on them and interaction with human serum albumin, *Food Chem.*, 2023, **424**, 136371.
38 K. Chan and A. Zinchenko, Aminolysis-assisted hydrothermal conversion of waste PET plastic to N-doped carbon dots with markedly enhanced fluorescence, *J. Environ. Chem. Eng.*, 2022, **10**, 107749.
39 M. M. Mikhail, H. B. Ahmed, A. E. M. Abdallah, M. El-Shahat and H. E. Emam, Surface passivation of carbon dots for tunable biological performance, *J. Fluoresc.*, 2024, DOI: 10.1007/s10895-024-03806-6.
40 M. Esmaeili Koutamehr, M. Moradi, H. Tajik, R. Molaei, M. Khakbaz Heshmati and A. Alizadeh, Sour whey-derived carbon dots; synthesis, characterization, antioxidant activity and antimicrobial performance on foodborne pathogens, *LWT*, 2023, **184**, 114978.
41 N. Rahmatian, S. Abbasi, N. Abbasi and M. Tavakkoli Yaraki, Alginate carbon dot nanocomposite: A green approach towards designing turn-on aptasenor for Candida albicans fungus, *Int. J. Biol. Macromol.*, 2024, **282**, 137315.
42 Y. Qu, S. Zhao, J. Ni, L. Jiao, X. Zhang, S. Benjakul, Z. Liu, X. Chen and B. Zhang, *In situ* formation mechanism of endogenous fluorescent carbon dots during the roasting process of small yellow croaker (Larimichthys polyactis), *Food Chem.: X*, 2025, **25**, 102187.
43 J. Bing, X. Xiao, D. J. McClements, Y. Biao and C. Chongjiang, Protein corona formation around inorganic nanoparticles: Food plant proteins-TiO2 nanoparticle interactions, *Food Hydrocolloids*, 2021, **115**, 106594.
44 Z. Zhong, S. Fang, Y. Li, Y. Huang, Y. Zhang, H. Chen, J. Zhang, H.-X. Wang, H. Xiong, Q. Zou and S. Wang, Quantitative analysis of protein corona on precoated protein nanoparticles and determined nanoparticles with ultralow protein corona and efficient targeting in vivo, *ACS Appl. Mater. Interfaces*, 2021, **13**, 56812–56824.
45 G. Mummaleti, J. Feng, A. Mohan, J. Suh, Z.-L. Kong and F. Kong, Microplastics interactions and transformations during *in vitro* digestion with milk, *Food Res. Int.*, 2024, **197**, 115247.
46 N. Barbero, M. Coletti, F. Catalano and S. Visentin, Exploring gold nanoparticles interaction with mucins: A spectroscopic-based study, *Int. J. Pharm.*, 2018, **535**, 438–443.
47 N. Archipowa, L. Wittmann, J. Köckenberger, F. J. Ertl, J. Gleixner, M. Keller, M. R. Heinrich and R. J. Kutta, Characterization of fluorescent dyes frequently used for bioimaging: photophysics and photocatalytical reactions with proteins, *J. Phys. Chem. B*, 2023, **127**, 9532–9542.
48 C. Wu, H. Dong, P. Wang, M. Han and X. Xu, Sequential changes in antioxidant activity and structure of curcumin-myofibrillar protein nanocomplex during in vitro digestion, *Food Chem.*, 2022, **382**, 132331.
49 M. Marczynski, T. M. Lutz, R. Schlatterer, M. Henkel, B. N. Balzer and O. Lieleg, Contamination with black carbon nanoparticles alters the selective permeability of mucin hydrogels: implications for molecular transport across mucosal barriers, *ACS Appl. Nano Mater.*, 2022, **5**, 16955–16970.
50 X. Qiao, L. Yang, J. Gu, Y. Cao, Z. Li, J. Xu and C. Xue, Kinetic interactions of nanocomplexes between astaxanthin esters with different molecular structures and β-lactoglobulin, *Food Chem.*, 2021, **335**, 127633.
51 M. Minekus, M. Alminger, P. Alvito, S. Ballance, T. Bohn, C. Bourlieu, F. Carrière, R. Boutrou, M. Corredig, D. Dupont, C. Dufour, L. Egger, M. Golding, S. Karakaya, B. Kirkhus, S. Le Feunteun, U. Lesmes, A. Macierzanka, A. Mackie, S. Marze, D. J. McClements, O. Ménard, I. Recio, C. N. Santos, R. P. Singh, G. E. Vegarud, M. S. J. Wickham, W. Weitschies and A. Brodkorb, A standardised static in vitro digestion method suitable for food-an international consensus, *Food Funct.*, 2014, **5**, 1113–1124.
52 H.-j. Zeng, J. You, H.-l. Liang, T. Qi, R. Yang and L.-b. Qu, Investigation on the binding interaction between silybin and pepsin by spectral and molecular docking, *Int. J. Biol. Macromol.*, 2014, **67**, 105–111.
53 X. Li, R. Xu, L. Shi and T. Ni, Design of flavonol-loaded cationic gold nanoparticles with enhanced antioxidant and antibacterial activities and their interaction with proteins, *Int. J. Biol. Macromol.*, 2023, **253**, 127074.
54 C. Yang, G. Xu, C. Hou and H. Zhang, Cobalt oxyhydroxide nanoflakes enable ratiometric fluorescent assay of gallic acid, *Food Chem.: X*, 2024, **24**, 101843.
55 Y. Wang, Y. Sun, J. Yang, L. Dai, N. Ji, L. Xiong and Q. Sun, Interactions of surface-functionalized starch nanoparticles with pepsin and trypsin in simulated gastrointestinal fluids, *J. Agric. Food Chem.*, 2020, **68**, 10174–10183.
56 H. B. Ahmed and H. E. Emam, Environmentally exploitable biocide/fluorescent metal marker carbon quantum dots, *RSC Adv.*, 2020, **10**, 42916–42929.
57 T. Sasikumar, J. S. Packialakshmi, S. J. Hong, S. Y. Ha, G. H. Shin and J. T. Kim, Multifunctional green-emitting fluorescent carbon dots: A versatile fluorometric probe for glyphosate detection and applications in food, *J. Environ. Chem. Eng.*, 2024, **12**, 113356.
58 H. Huang, H. Huang, J. Yang, H. Yang, J. Dai, Z. Li, W. Yao and X. Guo, Synthesis of P, N-dopped carbon nanosheets for highly sensitive fluorescence analysis of nitrofuran antibiotics in fish, *Food Chem.*, 2024, **459**, 140445.
59 Z. Zhang, F. Kong, H. Ni, Z. Mo, J.-B. Wan, D. Hua and C. Yan, Structural characterization, α-glucosidase inhibitory and DPPH scavenging activities of polysaccharides from guava, *Carbohydr. Polym.*, 2016, **144**, 106–114.
60 Y. Ogasawara, T. Namai, F. Yoshino, M.-C.-i. Lee and K. Ishii, Sialic acid is an essential moiety of mucin as a hydroxyl radical scavenger, *FEBS. Lett.*, 2007, **581**, 2473–2477.
61 A. Abodinar, K. Tømmeraas, E. Ronander, A. M. Smith and G. A. Morris, The physicochemical characterisation of pepsin degraded pig gastric mucin, *Int. J. Biol. Macromol.*, 2016, **87**, 281–286.
62 B. H. Sarmadi and A. Ismail, Antioxidative peptides from food proteins: a review, *Peptides*, 2010, **31**, 1949–1956.

63 A. W.-S. Zongo, D. Zogona, M. Youssef, S. Ye, F. Zhan, J. Li and B. Li, Senegalia macrostachya seed polysaccharides attenuate inflammation-induced intestinal epithelial barrier dysfunction in a Caco-2 and RAW264.7 macrophage co-culture model by inhibiting the NF-κB/MLCK pathway, *Food Funct.*, 2022, **13**, 11676–11689.

64 Y. Wu, X. Song, N. Wang, S. Cong, X. Zhao, R. Rai and M. Tan, Carbon dots from roasted chicken accumulate in lysosomes and induce lysosome-dependent cell death, *Food Funct.*, 2020, **11**, 10105–10113.

65 Y.-t. Li, K.-C. Mei, R. Liam-Or, J. T.-W. Wang, F. N. Faruqu, S. Zhu, Y.-l. Wang, Y. Lu and K. T. Al-Jamal, Graphene Oxide Nanosheets Toxicity in Mice Is Dependent on Protein Corona Composition and Host Immunity, *ACS Nano*, 2024, **18**, 22572–22585.

66 Y. Ji, Y. Wang, D. Shen, Q. Kang and L. Chen, Mucin corona delays intracellular trafficking and alleviates cytotoxicity of nanoplastic-benzopyrene combined contaminant, *J. Hazard. Mater.*, 2021, **406**, 124306.

67 D. Yang, D. Liu, M. Qin, B. Chen, S. Song, W. Dai, H. Zhang, X. Wang, Y. Wang, B. He, X. Tang and Q. Zhang, Intestinal mucin induces more endocytosis but less transcytosis of nanoparticles across enterocytes by triggering nanoclustering and strengthening the retrograde pathway, *ACS Appl. Mater. Interfaces*, 2018, **10**, 11443–11456.